Reversible Control of RNA Splicing by Photoswitchable Small Molecules

Lei Zhang, Xiulan Xie, Nemanja Djokovic, Katarina Nikolic, Dmitri Kosenkov, Frank Abendroth,* and Olalla Vázquez*

ABSTRACT: Dynamics are intrinsic to both RNA function and structure. Yet, the available means to precisely provide RNA-based processes with spatiotemporal resolution are scarce. Here, our work pioneers a reversible approach to regulate RNA splicing within primary patient-derived cells by synthetic photoswitches. Our small molecule enables conditional real-time control at mRNA and protein levels. NMR experiments, together with theoretical calculations, photochemical characterization, fluorescence polar-dependent exon inclusion as well as an increase in the target functional protein. Therefore, we first demonstrated the potential of photopharmacology modulation in splicing, tweaking the current optochemical toolkit. The timeliness on the consolidation of RNA research as the driving force toward therapeutical innovation holds the promise that our approach will contribute to redrawing the vision of RNA.

■ INTRODUCTION

Technological advances over the last decades led to the general acceptance that RNA is more than the messenger in charge of transferring the flow of genetic information from DNA to proteins. Indeed, RNA is a pivotal molecule of life. Now, it has become clear that the versatile RNA family, together with its regulatory machinery, are responsible for the optimal orchestration that determines human health.[1−3] Thus, a new paradigm focused on RNA manipulation has risen to expand druggability opportunities by addressing biological mechanisms as it has never been possible before. Such programmable action will ultimately correct or inhibit disease phenotypes. For instance, the breakthrough of mRNA vaccines against COVID-19 reasserts the prominent role of RNA for therapeutic intervention ranging from infectious to neurodegenerative diseases and even cancer.[4]

RNA executes complex functions at specific times and localizations; therefore, precise control over RNA dynamics is in high demand not only for deciphering the molecular mechanism underneath RNA-regulated systems but also for pharmacological application or diagnosis.[5,6] For this purpose, light-mediated approaches are invaluable because of their intrinsic spatiotemporal resolution with minimal invasive action. Although recent years have witnessed a growing fascination with using these tools to interrogate biological processes,[7,8] the toolkit for RNA photocontrol remains vastly underexplored.[6,9] In this context, modified oligonucleotides with either photoswitches[10−15] or photocages[16−18] have been effective; however, they require alterations in the native structure and suffer from metabolic degradation as well as uptake issues, above all, for crossing the blood−brain barrier. There are also a few examples of riboswitches or RNA aptamers[6] capable of selectively interacting with a conformer of a photoswitchable ligand[19,20] or photoreceptors.[21] Recently, this latter approach has evolved into entirely genetically encodable ones.[22,23] However, the emergence of small molecules as efficient RNA binders provides a timely starting point for developing optochemical tools that take full advantage of the small-molecule photoswitches.

Among the different RNA processes, splicing attracted our attention due to its potential for fine-tuning gene expression. As the last step of mRNA biosynthesis, splicing is responsible for the generation of different protein isoforms, which increases proteome diversity but can also lead to malfunctioning proteins or even prevent their production. Consequently, these undesirable events may, in turn, result in severe health disorders. Thus, deliberate manipulation of RNA processing

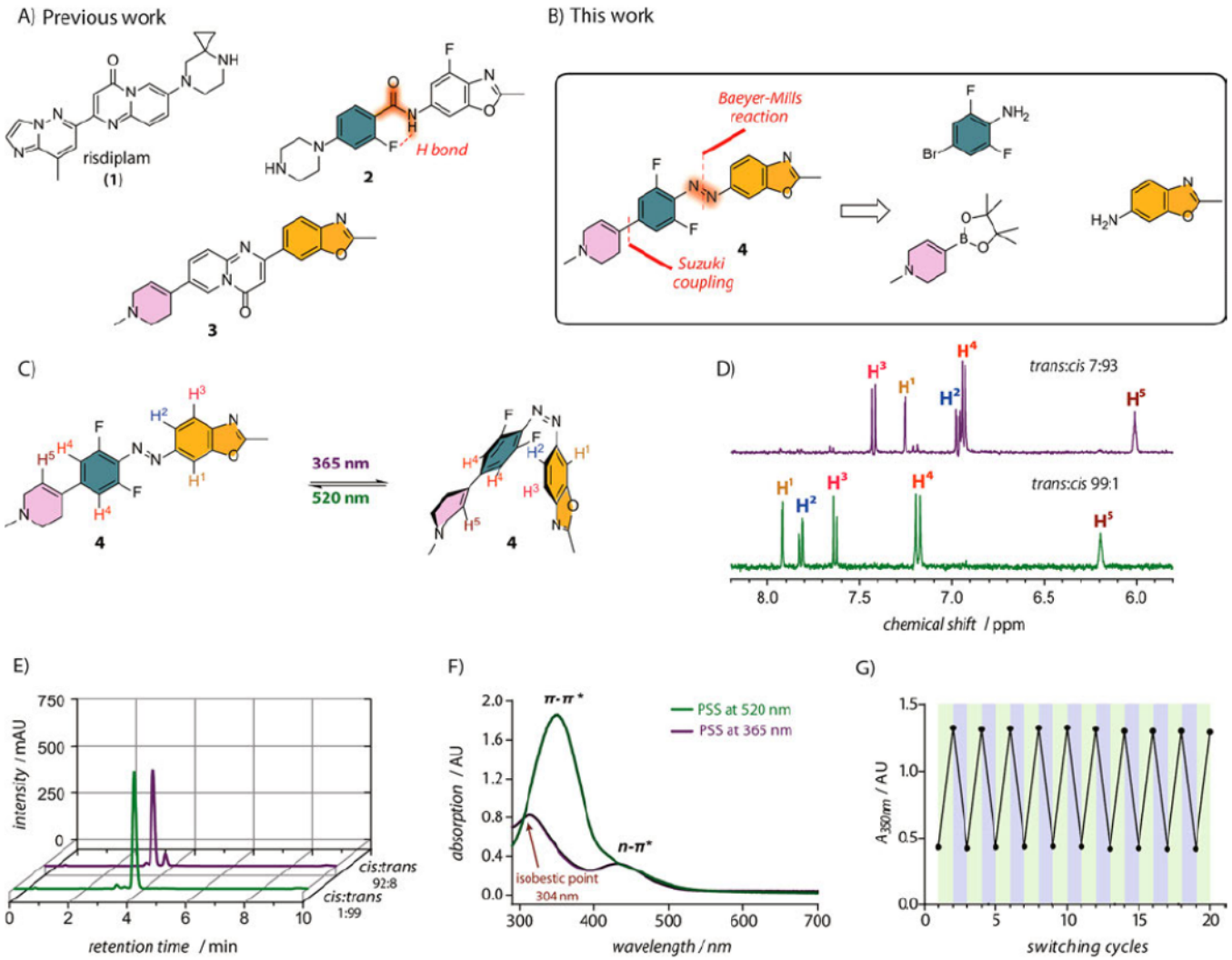

Figure 1. Precedents and photoisomerization studies. (A) Previous related structures. (B) Retrosynthesis of our novel compound 4. (C) Photoisomerization of 4. (D) Selected aromatic region of the ^{1}H NMR spectra (500 MHz) of a 100 μM solution of 4, without irradiation (green) and upon 365 nm irradiation for 1 min (purple) in phosphate buffer (10 mM NaH_2PO_4/Na_2HPO_4, 50 mM NaCl, 0.1 mM EDTA, at approximately pH 6.7 in H_2O/D_2O 9:1 with 5% of DMSO-d_6). (E) HPLC chromatogram of a 100 μM solution of 4 in ultrapure H_2O/MeCN (1:1), without irradiation (green) and upon 365 nm irradiation for 1 min (purple). (F) UV−vis spectra in an aqueous solution of 4 (50 μM) without and after irradiation at 365 nm for 1 min, reaching the photostationary state (PSS) in phosphate buffer (140 mM NaCl, 10 mM Na_2HPO_4, 2.7 mM KCl, 1.8 mM KH_2PO_4, pH 7.4). (G) Reversible *cis:trans* switching between photoisomers by alternating illumination at 365 (purple)/520 (green) nm for 1 min and 30 s, respectively, in phosphate buffer (140 mM NaCl, 10 mM Na_2HPO_4, 2.7 mM KCl, 1.8 mM KH_2PO_4, pH 7.4).

represents a powerful platform capable of controlling cellular homeostasis and restoring function in disease states. Since spatiotemporal regulation of splicing determines fundamental biological processes,[24] providing such a control layer for actual applicability is essential. Along these lines, the precise photocontrol of splicing to trigger phenotypic traits systematically will not only open unprecedented venues for the elucidation of the complex mechanisms underneath splicing but also induce noncanonical genetic outputs in a light-dependent manner. Notably, light-activated approaches toward reversible control of RNA splicing have not been explored, following the general tendency. Indeed, to our knowledge, previous research has only been limited to photocaged splice-switching oligonucleotides[25] and optogenetics using encoded splicing factors such as the arginine/serine-rich (RS) domain of SRS7 or the glycine-rich one or hnRNP-A1.[23] However, the field of photocontrol of molecular activity has evolved and recently placed photopharmacology[26,27] at its core.[28,29] Synthetic photoswitches can control functional responses in unmodified biological targets, bypassing the delivery of genes into target cells.[14,30] Therefore, this strategy holds promise to minimize off-target effects and resistance by on-demand therapeutic action. So, photoswitches have enabled reversible modulation of vision,[31] membrane transport,[32] *in vivo* enzymatic activity,[33] and cytoskeleton dynamics,[34] among others.[28,29] However, despite these advantages, there are no examples of photoswitches in the context of RNA editing nor in RNA splicing.

Herein, we first introduce photoswitchable RNA binders (K_d in the μM range) for reprogramming splicing under irradiation in living cells. Our photoswitchable splicing modifier enables switch-like responses at the mRNA level as well as the translational one. Moreover, we demonstrated that this methodology based on orally bioavailable molecules works even with primary patient fibroblasts. Importantly, our proof-of-concept sets the scene for game-changing technologies

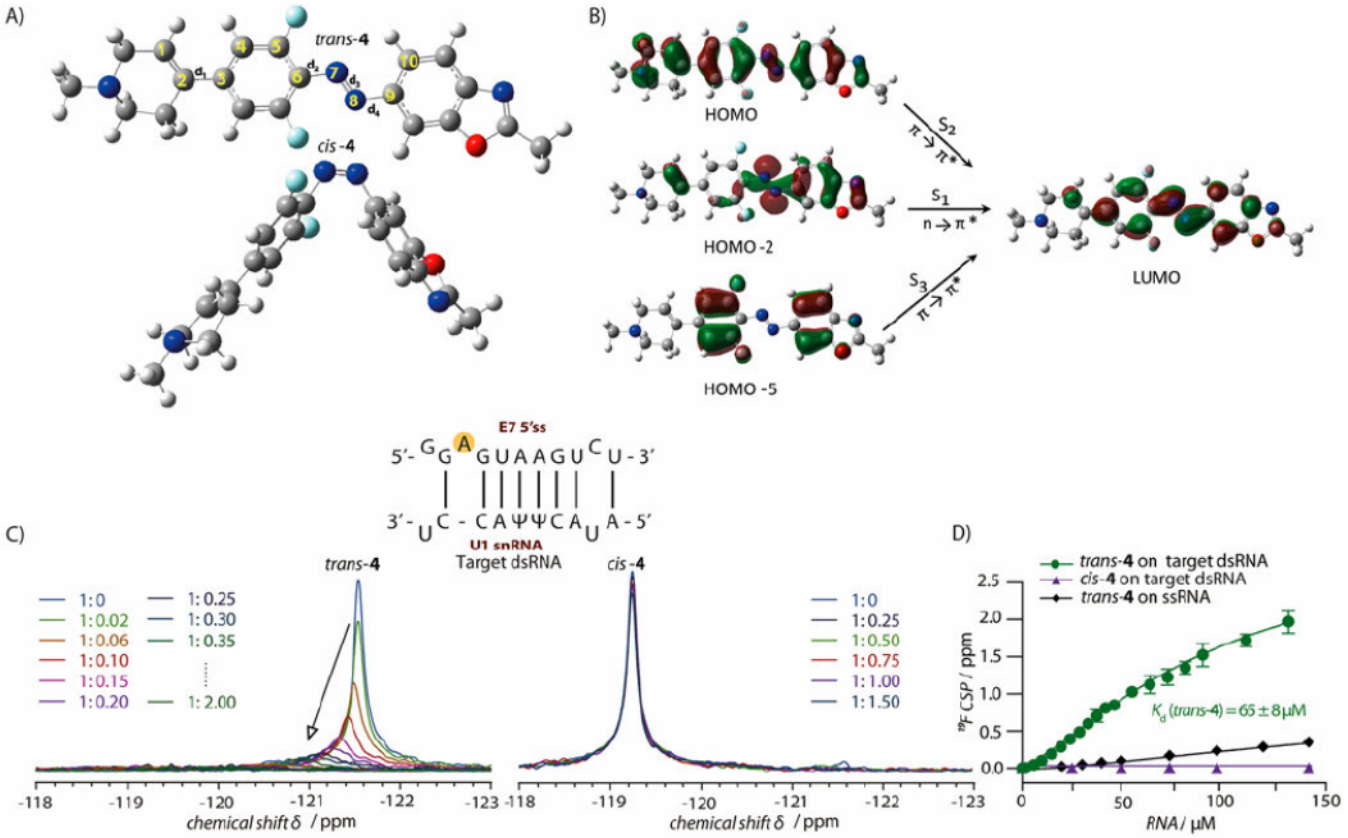

Figure 2. Computational results on the ligand 4 and NMR data on direct interactions of the ligand with dsRNA. (A) Molecular structures of *trans* and *cis* conformations and definitions of the dihedral angles d_1−d_4 of the ligand 4 (see also Tables S22 and S24). (B) Molecular orbitals that make major contributions to the lowest three singlet electronic transitions (S1−S3) of the ligand 4 (see also Table S23). (C) Overlay of ^{19}F spectra of titrations of either a 100 μM solution of *trans*-4 (left) or *cis*-4 (right) with increasing concentrations of target dsRNA in phosphate buffer (10 mM NaH_2PO_4/Na_2HPO_4, 50 mM NaCl, 0.1 mM EDTA, at approximately pH 6.7 in H_2O/D_2O 9:1 with 5% of DMSO-d_6). The spectra are colored according to 4:target dsRNA ratios indicated in the panel. (D) Plot of the ^{19}F chemical shift perturbation (CSP) observed for *trans*-4 (green) and *cis*-4 (purple) on target dsRNA (U1 snRNA: AUAC Ψ ΨUACCUG/E7 5′ ss: GGAGUAAGUCU; Ψ: pseudouridine) and *trans*-4 on ssRNA E7 5′ ss (black) as a function of the RNA concentrations. Mean data points and standard deviations are derived from two independent experiments.

based on RNA-mediated processes[35] toward precise light-inducible delivery of any phenotypic response in living organisms, which will provide unprecedented opportunities in gene therapy.

■ RESULTS AND DISCUSSION

Design and Photochemical Evaluation. Inspired by the approval of the oral splicing modifier risdiplam[36] (**1**, commercialized under the name Evrysdi, Figure 1A) for the treatment of spinal muscular atrophy (SMA) in 2020, we envisioned exerting light-controllable manipulation in RNA splicing to modulate survival motor neuron (SMN) protein levels, which is the molecular target of SMA. SMA is an incurable neuromuscular disease where the C-to-U transition on exon 7 of the gene SMN2 causes exon skipping and, consequently, an aberrant variant.[37] Less than 10 years ago, different laboratories reported small molecules capable of specifically including 7 exon and restoring the healthy levels of SMN. In particular, the derivatives **2**[38] and **3**[39] called our attention (Figure 1A). Thus, the exchange of the fused bicyclic scaffolds by a fluorobenzamide group minimized toxic side effects while retaining potency. Importantly, the fluorine atom locks the quasi planar active conformation via an intramolecular hydrogen bond. The fact that the planarity is essential for the activity suggests a plausible foundation for achieving azobenzene-induced RNA splicing. Generally speaking, *ortho*-fluorine functionalization of azobenzene retains the difference in planarity between isomers while it surpasses the photochemical properties of classical azobenzenes.[40] Furthermore, amide bonds are well suited to azologization.[41] Taking all together, we designed the azobenzene derivative **4**, which contains the presumable photoswitching 2,6-difluorophenyldiazenyl group. This molecule can be straightforwardly synthesized in two steps, i.e., the classical Baeyer−Mills reaction between 2-methyl-6-amino-benzoxazole and 4-bromo-2,6-difluoro-nitrosobenzene followed by a Suzuki−Miyaura coupling of the azo-derivative with the corresponding boronic acid pinacol ester for functionalization.

Once the compound was synthesized, we evaluated its photochemical performance. As in the classical unsubstituted azobenzenes,[42] the *trans*-isomer is the thermodynamically most stable. The maximum amount of the *trans*-isomer (>99%) was directly obtained with a freshly prepared sample in the dark (Figures 1D,E and S14), whose UV−vis spectrum displayed the characteristic high-energy band assigned to the $\pi \rightarrow \pi^*$ transition, with λ_{max} = 349 nm (Figure 1F). The wavelength dependency of the photostationary ratios was investigated in detail (Table S13 and Figure S9). Notably, irradiation at 365 nm surpassed the *cis*:*trans* ratio of classical azobenzenes, reaching 90%, or more, of the *cis*-isomer in phosphate buffer

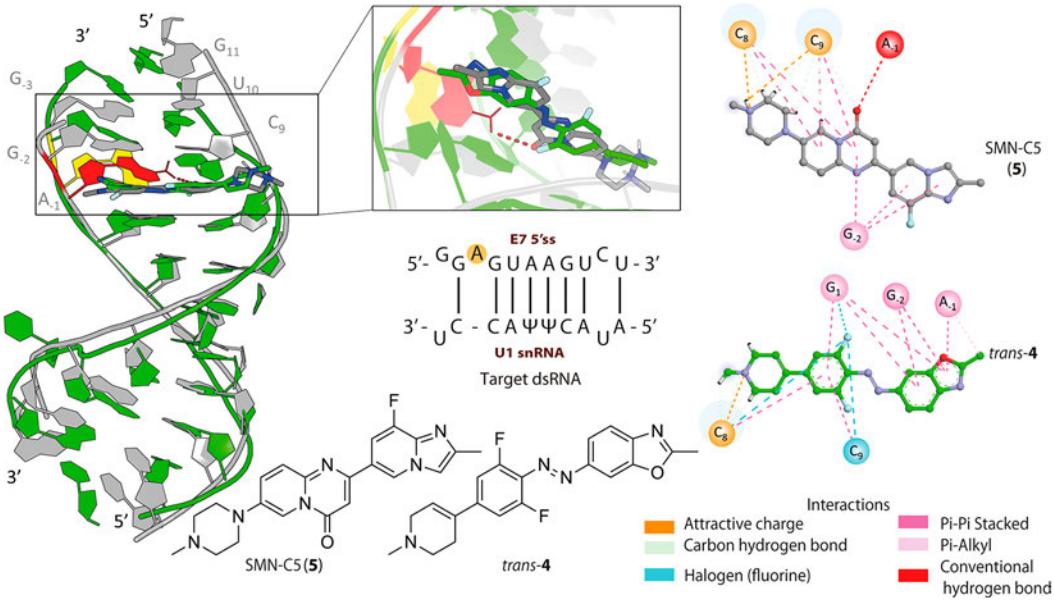

Figure 3. Comparison of binding modes of *trans*-4 (green sticks and cartoon) and SMN-C5 (**5**, gray sticks and cartoon). Left: Bulged adenine (A_{-1}) is represented in yellow (dsRNA: *trans*-4) or in red (dsRNA: SMN-C5). Red dashed line in 3D representation indicates an H-bond. Right: Interactions of specific ligands are depicted in 2D plots.

pH 6.7 or pH 7.4, according to NMR (Figure 1D) and HPLC (Figure S14) measurements at the photostationary state (PSS), respectively. While the NMR buffer reproduced the one used with pseudouridine-containing dsRNA,[43] the latter one mimics physiological conditions in an attempt to have transferable results for possible biological experiments. The *cis*-to-*trans* backswitching was less efficient, reaching approximately 55% at 520 nm (58% at 455 nm) of the *trans*-isomer in a 1:1 mixture of ultrapure H_2O/MeCN (Figure S9). However, both its half-life and photoswitching reversibility were excellent; that is, minimal isomerization changes were detected by NMR (Figure S13) as well as HPLC (Figure S14). Rapid photoswitching was monitored up to 20 cycles without signs of degradation (Figure 1G). Furthermore, the *cis*-isomer was stable to thermal relaxation: 74% of the *cis*-isomer in phosphate buffer (pH 6.7) after 2 days and 77% after 24 h (pH 7.4) (Figures S13 and S14).

After the demonstration of the switching properties of **4**, we performed quantum chemical calculations (Tables S22−S24) to explore photoinduced molecular changes by simulating molecular structures of *trans*- and *cis*-isomers. The molecular geometry of the ligand **4** is described by the dihedral angle (Figure 2A) d_1 (C1═C2−C3═C4) that determines orientation of the *N*-methyl-tetrahydropyridine with respect to the difluorophenyl group and d_2 (C5═C6−N7═N8) that determines orientation of the difluorophenyl with respect to the azo group (N7═N8). The dihedral angle d_3 (C6−N7═N8−C9) defines *cis* and *trans* conformations of the ligand **4**. Finally, the dihedral angle d_4 (N7═N8−C9═C10) determines the orientation of the benzoxazole with respect to the azo group. After the geometry optimization, it was found that both *cis* ($d_3 = -7°$) and *trans* ($d_3 = -179°$) conformers of the ligand **4** have four rotamers that differ in mutual orientations of the *N*-methyl-tetrahydropyridine and benzoxazole groups (Table S22). In both *cis* and *trans* conformations, the *N*-methyl-tetrahydropyridine and difluorophenyl group are almost in plane with each other within 30° based on the values of the d_1 dihedral angle. Difluorophenyl and azo groups are out of plane by up to 23° (dihedral d_2), and benzoxazole and azo groups are out of plane only by 3° (dihedral d_4) in the *trans* conformation of the ligand **4**. Thus, one can conclude the overall planarity of the *trans* conformation. On the contrary, the *cis* conformation is substantially nonplanar (Figure 2A, Table S24). Additionally, benzoxazole is out of plane with respect to the azo group by 47−54° (dihedral d_4). The thermochemical calculations show that in the electronic ground state the planar *trans* conformation is more stable by 8 kcal/mol as compared to the nonplanar *cis* conformation for all considered rotamers (Table S22). Therefore, our calculations suggested that the twisted *cis*-isomer is likely not present in the equilibrium mixture, whereas a more stable *trans*-analogue is dominating in the equilibrium mixture. The *trans*-isomer is also more likely to interact with RNA due to its nearly planar geometry.

Mechanisms of photoisomerization of azobenzene and its derivatives were a subject of numerous studies.[44−51] It was previously shown that the *trans* → *cis* photoisomerization upon UV irradiation proceeds via torsional, inversion photoisomerization pathways or their combinations and is dependent on the wavelength of the radiation.[47] In the present study, the irradiation with UV light (365 nm) is likely leading to the excitation of the *trans*-isomer to the S_2 excited state. Our calculations (Table S23) suggest that the S_2 state corresponds to the $\pi \rightarrow \pi^*$ HOMO−LUMO transition (Figure 2B) with the vertical excitation energy 335 nm (which is close to that experimentally measured). The absorption of UV light is also likely leading to the excitation of the S_2 state due to large oscillator strength (1.5) of the $S_0 \rightarrow S_2$ transition as compared to other considered transitions. Then, the S_2 relaxes to a lower lying S_1 $n \rightarrow \pi^*$ state and subsequently decays through the S_1/S_0 conical intersection[47] to the ground state S_0. The decay to the ground state occurs along the d_3 dihedral angle rotation (torsional pathway) close to ∼90.0°.[48,50,51] The high yield (92%) of the *cis* form in this process suggests that this torsional pathway is dominating over the in-plane inversion pathways that usually produce lower yields of the *cis* form.[44] In our

study, the *cis* → *trans* back isomerization upon irradiation at 520 nm green light resulted in only 55% of the *trans*-isomer formed. The photochemical mechanism of this back isomerization is not completely clear. It is possible that initial excitation of the S_1 n → π^* state (at 433 nm calculated and 430 nm experimentally measured) of the *cis* form with a subsequent torsional isomerization and potential decay via S_1/S_0 conical intersection.[47,50] Thus, we speculate that in both cases of the *trans* → *cis* and back isomerization there is an apparent difference from the isomerization mechanism of azobenzene,[44] which is likely due to partial or complete unavailability of the inversion pathway in the ligand 4.

Light-Dependent RNA Binding. Mechanistic studies for the parental compounds demonstrated two separated binding sites (1 and 2) in exon 7 of the SMN2 pre-mRNA.[52] Thus, one of the modes of action involves dsRNA recognition (binding site 1).[53−55] Here, exon 7 inclusion is achieved by the stabilization of the double-stranded (ds)RNA formed by the 5′ splice site (SS) of the SMN2 exon 7, and the U1 snRNA, together with induced conformational changes upon binding, was suggested.[56−58] Of note, the terminal stem-loop 2 (TLS2) sequesters the 5′SS of exon 7 in SMN2.[59] Using the same binding target (Figure 2C) we investigated if our photoswitchable molecules retain the parental binding capacities and if the azologization provides RNA interaction in a light-controlled manner. We monitored the direct binding of both isomers to the RNA duplex using ^{19}F NMR spectroscopy. The stepwise addition of the target dsRNA to the *trans*-4 displaced its ^{19}F signal to downfield shift, which corroborated the interaction and enabled the determination of its affinity (K_d = 65 ± 8 μM). Importantly, under the same conditions, the ^{19}F signal of the *cis*-isomer was imperturbable, and, consequently, no binding to dsRNA was detectable. As expected from the precedents of the risdiplam derivatives, dsRNA was necessary for recognition that involves the binding site 1 (Figure 2D). Next, molecular docking and molecular dynamic (MD) simulations were used to shed light on the binding of 4 to the dsRNA (Figure 3) Molecular docking calculations with the previously published structure of the dsRNA:SMN-C5 complex (PDB ID: 6HMO)[54] were utilized for initial predictions of the binding modes of 4. Further refinement of the predicted binding modes, together with assessment of dynamics of the dsRNA:4 complexes, was performed by the means of MD simulations. Root mean square deviation (RMSD) analysis of obtained trajectories for apo dsRNA, dsRNA:SMN-C5, and dsRNA:*trans*-4 indicated well stabilized systems during the course of simulation (Figure S40), while visual analysis of dsRNA:SMN-C5 and dsRNA:*trans*-4 trajectories indicated resemblance of the *trans*-4 predicted binding mode to the binding mode of SMN-C5 (5) (Figure 3). The positively charged tetrahydropyridyl group of *trans*-4 displayed the same electrostatic interactions with the phosphate group of C_8 as the positively charged pyperazine group in SMN-C5 (5) (Figure 3). However, the absence of the pyridopyrimidinone core in our photoswitchable ligand prevented the H-bond between the carbonyl oxygen of SMN-C5 (5) and the bulged adenine at the exon−intron junction (A_{-1}), which were considered key for the proposed SMN-C5 binding mechanism. Instead of hydrogen bonding, the benzoxazole moiety of *trans*-4 achieved numerous π−π stacking interactions with A_{-1}, G_{-2}, and G_1 at the exon−intron junction (Figure 3). Principal component analysis (PCA) showed a conformational difference between the apo dsRNA and studied holo systems, while suggesting the similar conformational behavior of dsRNA:SMN-C5 and dsRNA:-*trans*-4 systems (Figure S41). Analysis of conformational differences between apo and holo structures indicated particular changes in the G_{-3}, G_{-2}, A_{-1}/G_{11}, U_{10}, and C_9 segment of dsRNA, which was in accordance with the literature data (Figure S41).[54] This was further corroborated by H-bond analysis of dsRNA, which indicated an increased number of H-bonds in of the G_{-3}, G_{-2}, A_{-1}/G_{11}, U_{10}, C_9 segment upon SMN-C5 and *trans*-4 binding (Figures S43−S45).

The binding site 2 belongs to the exonic splicing enhancer (ESE) 2.[56] This single-stranded (ss)RNA sequence is a purine-rich one located approximately 24 nucleotides upstream of the 5′ SS. Previous fluorescence polarization (FP) measurements of the compound SMN-C2 (6) in magnesium-containing HEPES buffer indicated preference for the synthetic ssRNA that contains the putative sequence 5′-AGGAAG-3′ (K_d = 24.3 ± 2.31 μM for $ssRNA_{BS2A}$, Figure S37).[53] By competitive FP experiments, we demonstrated that our *trans*-4 can efficiently displace the coumarin derivative 6 with an apparent K_i of 8.24 ± 0.73 μM, while the *cis*-4 cannot (Figure 4). As reported for

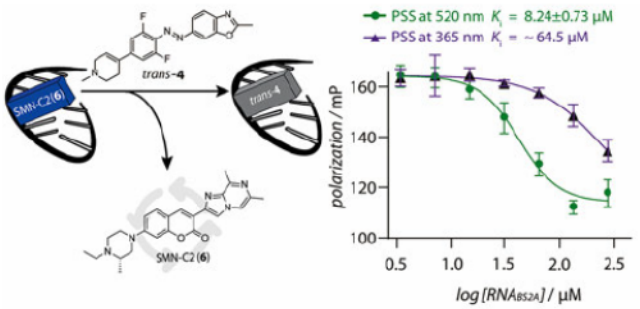

Figure 4. Competitive fluorescence polarization assays. Left: Schematic representation of the experiment. Right: Dose−response curve of 4 at different photostationary states in the presence of 200 nM SMN-C2 (6) and 25 μM ssRNA binding site 2A ($ssRNA_{BS2A}$): 3′-AGAAGGAAGGUGCUC-5′ in 100 mM HEPES, 300 mM NaCl, 8 mM $MgCl_2$, pH = 7.4. Mean data points and standard deviation are derived from three independent experiments.

SMN-C2 (6),[53] our compound could also bind to the 5′SS exon with a similar sequence (5′-AAGGAG-3′) to the target one, i.e., $ssRNA_{BS2B}$ (Table S21). Once again, the interaction depended on the PSS (Figure S38). Of note, the FP polarization procedure did not affect the photoisomerization ratio (Figure S39).

Taken all together, we propose that our light-controllable RNA binder 4 shares the dual recognition mode of risdiplam. On the one hand, both NMR and calculations suggest that stabilization of the bulged adenine A_{-1} occurs upon binding of the *trans*-4. Notably, all our attempts to simulate the *cis*-4 bound to the target dsRNA failed in the determination of a stable binding pose, identifying this isomer of 4 as a weak binder (Figure S42). Consequently, these results are in concordance with our NMR experiments. On the other hand, competitive FP experiments showed a direct binding to the GA-rich sequence of the ESE. Although we used two different techniques to determine the affinity, i.e., FP and NMR chemical shift assays, the obtained K_d values for *trans*-4 are generally consistent with the reported values for SMN splicing modifiers. In particular, Campagne et al.[54] determined

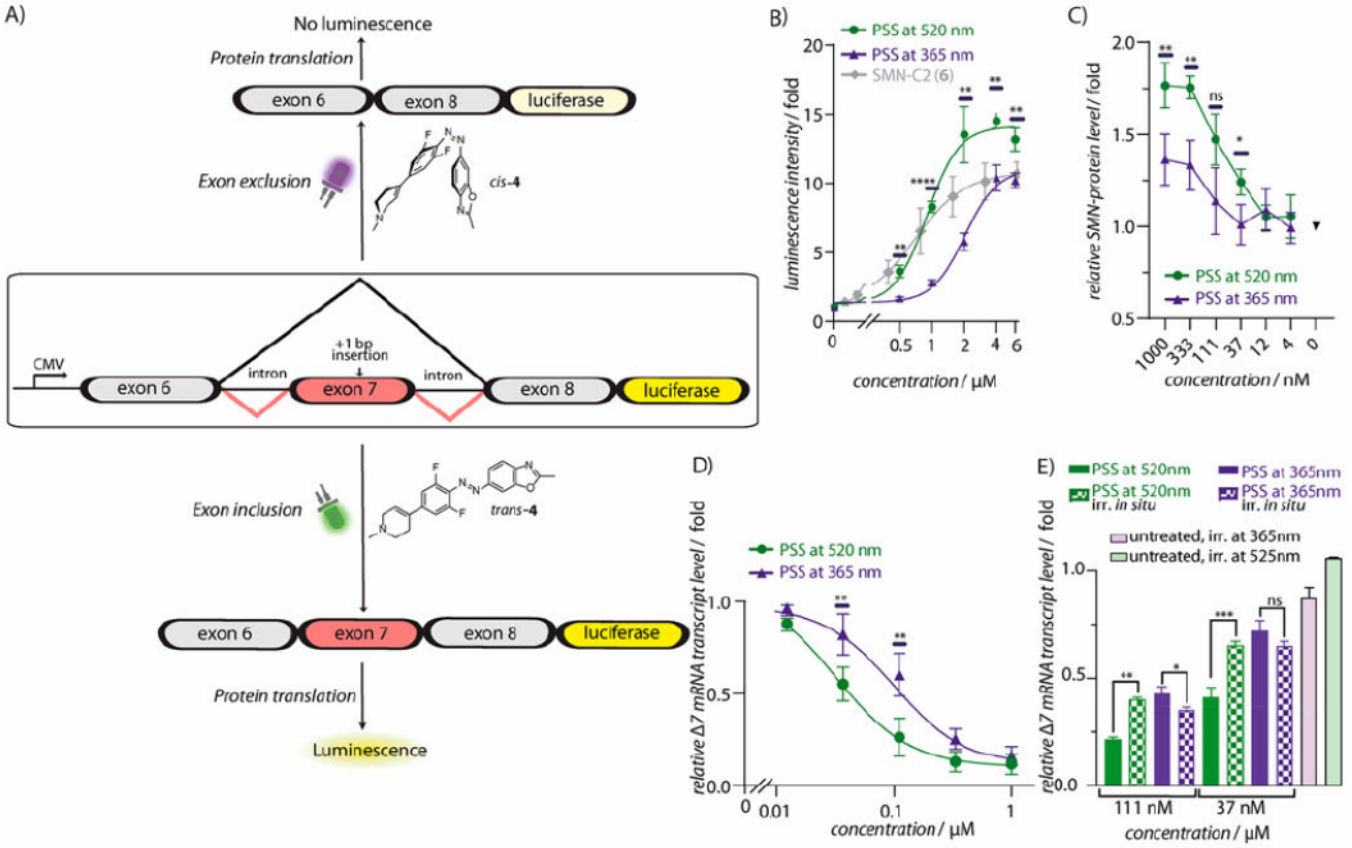

Figure 5. Light-dependent exon inclusion experiments. (A) Schematic representation of the transfected SMN2 reporter construct in HEK293T cells and mechanism of action of **4**. The firefly luciferase gene is highlighted in yellow (B) Dose–response curve of **4** at different photostationary (PSS) states in HEK293T cells and SMN-C2 (**6**). The luciferase assay was performed 6 h after incubation of the corresponding PSS of **4** and SMN-C2 (**6**). Mean data points and standard deviations are derived from three independent experiments; $^{****}p < 0.0001$, $^{**}p < 0.01$, $n = 3$. Concentration-dependence data were fitted to a Hill equation. (C) HTRF analysis of SMN protein in GM03813 primary patient fibroblasts after 48 h of treatment with different concentrations of *trans*-**4** (green) and *cis*-**4** (purple). Mean data points and standard deviations are derived from three independent experiments; $^{*}p < 0.05$, $^{**}p < 0.01$, ns = nonstatistically significant, $n = 3$. (D) RT-qPCR quantification of relative *SMN*Δ7 mRNA expression levels in SMA type I patient fibroblasts (GM03813) after 6 h of incubation with the corresponding PSS of **4** at different concentrations and standardized to the endogenous GAPDH control. Mean data points and standard deviations are derived from three independent experiments; $^{**}p < 0.01$, $n = 3$. Concentration-dependence data were fitted to a Hill equation. (E) Effect of *in situ* photoisomerization of **4** after 6 h of incubation in GM03813, including *in situ* irradiation (60 s at 365 nm for the PSS at 520 nm and 180 s at 525 nm for the PSS at 365 nm) in the middle of incubation (3 h) on *SMN*Δ7 transcript levels by RT-qPCR analysis at 111 and 37 nM. Mean data points and standard deviations are derived from three independent experiments; $^{*}p < 0.05$, $^{**}p < 0.01$, $^{***}p < 0.001$, ns = nonstatistically significant, $n = 3$. CMV: human cytomegalovirus promotor; bp: base pair.

the affinity of SMN-C5 (**5**) to the same dsRNA (binding site 1) as K_d = 28 μM by ^{19}F NMR chemical shift assays. SPR assays with an ssRNA containing the binding site 2 (5′-AAGAAGGAAGGUGC-3′) showed a value of 8.0 μM, according to Tang et al.[52] Other splicing modifiers such as SMN-CX and SMN-CY displayed K_d values of 74 and 60 μM, respectively, to the dsRNA binding site 1 by NMR chemical shift assays.[54] As mention before, the coumarin derivative SMN-C2 (**6**) showed K_d values of 24 μM to the ssRNA binding site 2[53] and 60 μM to the dsRNA binding site 1.[52] Finally, other coumarin analogues presented affinities from 18.5 μM up to >100 μM in the presence of an ssRNA, which contains one single mismatch in the binding site 2 (5′-AAAAGAAGGAGGGTGCTC-3′).[52] Therefore, our data are in agreement with the literature and indicated a stronger interaction for the binding site 2 than 1.

Environment can affect photoisomerization.[60] Consequently, once the RNA binding was confirmed, we performed *in vitro* photoswitching experiments in the presence of the ssRNA$_{BS2A}$. While the equimolar presence of the target ssRNA hardly affected both photoisomerization ratios (Figures S14 and S15) and the thermal lifetime for *cis*-**4** (Figures S14 and S15), the quantum yields clearly decreased upon RNA addition ($\Phi_{trans\rightarrow cis}$ = 0.425 ± 0.014 without RNA versus 0.205 ± 0.007 with RNA; $\Phi_{cis\rightarrow trans}$ = 0.319 ± 0.015 without RNA versus 0.142 ± 0.007 with RNA). Along these lines, photoisomerization rate is slower with RNA. Thus, in the absence of RNA 40 and 20 s are enough for reaching the PSS either at 365 nm or at 520 nm, respectively. However, in the presence of RNA the same time is necessary with less than half of the concentration (Figures S10 and S11).

Luciferase Reporter Assays and RT-qPCR in Primary Fibroblasts Reveal SMN2 Exon 7 Inclusion. The direct RNA interaction of *trans*-**4** and the *in vitro* differences in the RNA binding capacities between isomers encouraged the assessment of SMN2 exon 7 inclusion activity in a cellular setting. Toward this end, we established a luciferase reporter gene-based assay in HEK293T cells (Figure 5A). In our design

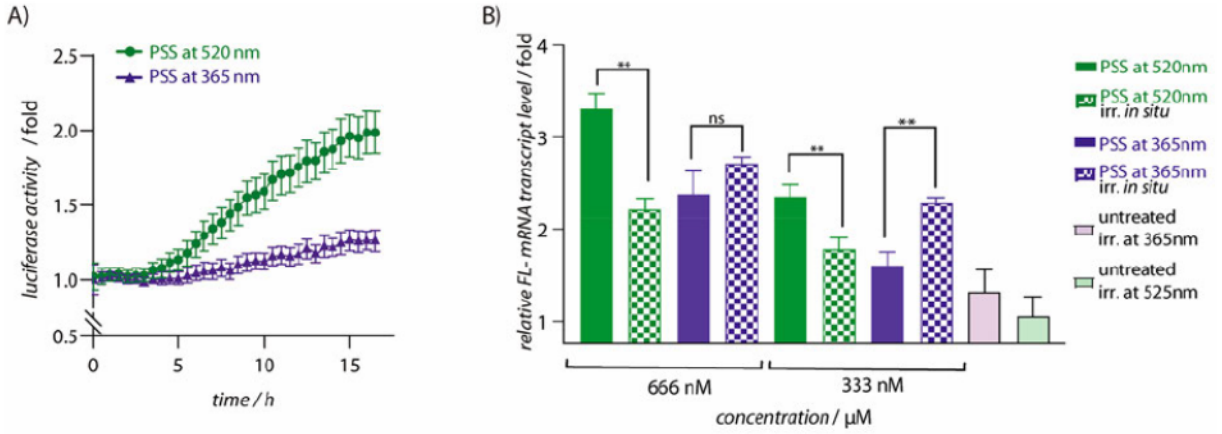

Figure 6. Monitoring temporal response to both rapid and transient alterations in protein SMN2-NLucP expression in HEK293T cells. (A) Live real-time expression of SMN protein in HEK293T cells in the presence of 313 nM of *trans*-**4** (green) and *cis*-**4** (purple) using NLucP as reporter and 25 μM endurazine. NLucP protein expression levels were normalized as protein levels of untreated cells. Plot represents mean data points of three independent measurements with corresponding standard deviations. (B) Effect of reversible photoisomerization of **4** after 6 h of incubation with *in situ* irradiation (60 s at 365 nm for the PSS at 520 nm and 180 s at 525 nm for the PSS at 365 nm) in the middle of incubation (3 h) on *FL-SMN* transcript levels in HEK293T-SMN2-NLucP cells determined by RT-qPCR analysis. Mean data points and standard deviations are derived from three independent experiments; $^{**}p < 0.01$, nonstatistically significant $n = 3$.

the reporter is only in-frame when exon 7 is included because of a described single-point mutation.[61] Thus, we constructed an SMN2 minigene (SMN2-Luc) comprised of the exon sequences: 6 to 8 fused to the red firefly luciferase one at the 3′ end of the exon 8 reading frame. Depending on the behavior of the exon 7 during splicing, two mRNA isoforms can be generated (Figure 5A): (1) the exon 7-skipped transcript (*SMN*Δ7) when exon 6 is spliced onto exon 8 with the out-of-frame luciferase gene and (2) the full-length transcript (FL-*SMN*) when exon 7 is included. Translation of the latter transcript (FL-*SMN*) provides the luciferase fusion protein, whose activity is, therefore, proportional to the exon 7 inclusion activity. The treatment of the stable transfected SMN2-Luc HEK293T cells with **4** led to a luminescence increase in a dose−response fashion (Figure 5B), despite its moderate RNA affinity. Indeed, it is also possible that our molecule **4** impacts RNA:protein interactions as it was described for SMN-C2 (**6**) and hnRNP G/FUBP1/KHSRP,[53] or even different ones. However, these further mechanistic studies to elucidate the complete mode of action of our photoswitchable splicing modifier are beyond the scope this work. Importantly, the protein increase was significantly (***, $p < 0.001$) higher for the *trans*-**4** without affecting the cell viability (Figure S19). These observations are in concordance with the *in vitro* experiments as well as the calculations. Comparing SMN2 induction of *trans*-**4** to other splicing modifiers such as SMN-C2 (**6**) (Figure 5B) and the commercially available branaplam (**7**, also known as NVS-SM1 and LMI070; Figure S24)[62] and risdiplam (**1**, Figure S24),[36] the protein increase is higher for those compounds with a dual recognition mode of action, i.e., risdiplam (**1**), SMN-C2 (**6**), and *trans*-**4**. Except for risdiplam (**1**), our *trans*-**4** caused the highest protein increment among the tested compounds whose EC_{50} of 899 ± 87 nM is comparable to the one for SMN-C2 (**6**) (Figure 5B and Table S15).

To ensure that the observed signal comes from the **4**-mediated exon 7 inclusion, we conducted homogeneous time-resolved fluorescence (HTRF)[63] and quantified mRNA transcript levels by quantitative reverse transcription polymerase chain reaction (RT-qPCR) in a primary SMA-patient fibroblast cell line (GM03813). These primary fibroblasts carry no functional SMN1 gene and only two copies of the SMN2 gene derived from patients who suffered the most severe case of SMA (SMA type I); consequently, they are an excellent proof to test if our molecule is able to alter alternative splicing levels and protein translation in a disease-relevant phenotype. Our compound induced an increase of SMN protein levels in primary fibroblast cells in a dose-dependent manner (Figure 5C). Of note, differences between isomers were observed, and *trans*-**4** was, once again, the isomer that generated the highest amount of SMN.

Regarding mRNA, gratifyingly, *SMN*Δ7 levels decreased while FL-*SMN* ones concomitantly increased with incrementing amounts of **4**. Importantly, we detected distinct differences in the transcript quantification of both mRNA (Figures 5D and S31) depending on the isomer; *trans*-**4** was the most potent splicing modulator. As expected,[64] isomer-dependent differences were more significant for the relative decrease of SMNΔ7 (Figure 5D versus Figure S31). In particular, while *trans*-**4** achieved a 75% decrease in *SMN*Δ7 relative expression at 111 nM in comparison with nontreated cells using the housekeeping gene GAPDH as reference, the *cis* analogue reached only 40% (Figure 5D).

Having a photoswitchable splicing modulator enables reversible control of mRNA levels. For this purpose, once the **4** isomers reached the corresponding PSS, these solutions were added to the fibroblasts (Figure 5E) followed by a brief *in situ* photoisomerization step, which means 60 s at 365 nm for the PSS at 520 nm and 180 s at 525 nm for the PSS at 365 nm in the middle point (3 h) of the total incubation (6 h). According to our *in vitro* experiments, we expected that this *in situ* irradiation is enough to change the PSSs (Figures S10 and S11) without hardly affecting cell viability (Figures 5E and S21). Importantly, a clear switching of the amount of mRNA was detected (Figures 5E and S31) as a consequence of **4** treatment.

Conditional Real-Time Temporal Control at both mRNA and Protein Levels. After demonstrating light-switching exon-inclusion activity at the mRNA level, we tested the applicability of our system in a scenario suitable for live-cell

kinetics (Figure 6). Thus, we designed an analogous reporter-gene assay where the red firefly luciferase was exchanged by the engineered NanoLuc luciferase[65] appended to a human protein degradation signal PEST (NLucP).[66] The inclusion of the PEST sequence should facilitate enzyme destabilization[67] and, therefore, shorten its half-life. First, we validated the activity of the assays with the addition of the commercial branaplam (7), which demonstrated clear inducibility upon branaplam addition in both cases (Figures S29 and S30). Besides, in these comparative experiments the new version, NLucP, increased the rate of destabilization of the reported protein (half-life time: ~7 h for the firefly luciferase versus ~2 h for the NanoLuc one (Figures S29 and S30)) under conditions of translation arrest with cycloheximide. In contrast, without the cycloheximide pretreatment no signal decrease was detected for at least 14 h. Next, we investigated if our compounds could offer temporal resolution in both transcription and translation. We monitored the time-course of the exon inclusion at different concentrations of our isomers measuring the intracellular luminescence derived from the NLucP enzyme. After 5 h of stimulation with *trans*-4, a persistent luminescence increased over at least 16 h, while the *cis*-4-induced signal was always lower (Figures 6A and S26). This kinetic behavior was consistent in all concentration−response measurements (Figure S27), having the largest induced increase at 313 nM of 4-*trans* (Figure 6A). To ascertain whether the here-observed induction of luminescence reflects mRNA transcriptional activity, we further conducted RT-qPCR experiments. These confirmed higher levels of the FL-*SMN* transcript in the presence of the *trans*-isomer (Figure 6B). Importantly, *in situ* irradiation enabled activity switching of 4 depending on PSSs. A significant switch of the expression level of FL-*SMN* mRNA in HEK293T cells was observed. These results are consistent with the ones on primary cells.

CONCLUSIONS

Light-responsive molecular technologies for RNA control remain in their infancy. Along these lines, photoswitches are mainly used in the context of protein function. Inspired by the drug risdiplam, here we introduce the first small molecule capable of achieving reversible photocontrol of RNA splicing to our knowledge. Our photoswitchable splicing modifier represents a useful tool for the control of both transcription and translation with high temporal resolution, even in the authentic scenario of primary patient cells. Cellular changes with temporal resolution were demonstrated too. With our proof-of-concept work in place, our toolkit could be easily implementable to other systems and become a universal switch element for fine-tuned gene regulation in a straightforward and quantitative fashion. In fact, conditional control of splicing is key for innovative therapeutic intervention,[68,69] and further applications based on our approach are expected. Consequently, we believe that our results open a new wave in the field of RNA chemistry, where the emergence of small molecules as efficient RNA binders, together with technological advances, will enable us to exploit uncharted territories in the field of chemistry and photopharmacology.

ASSOCIATED CONTENT

Supporting Information

The Supporting Information is available free of charge at https://pubs.acs.org/doi/10.1021/jacs.3c03275.

Experimental section and methods including general procedures of UV−vis characterization, photoisomerization, cell-based assays, NMR binding affinity, modeling including a PDB file and quantum chemical calculations as well as supplementary figures and tables (PDF)

AUTHOR INFORMATION

Corresponding Authors

Frank Abendroth − *Department of Chemistry, University of Marburg, Marburg D-35043, Germany;* orcid.org/0000-0002 0320 2690; Email: abendrot@staff.uni marburg.de

Olalla Vázquez − *Department of Chemistry and Center for Synthetic Microbiology (SYNMIKRO), University of Marburg, Marburg D-35043, Germany;* orcid.org/0000-0002-7555-1865; Email: olalla.vazquez@staff.uni-marburg.de

Authors

Lei Zhang − *Department of Chemistry, University of Marburg, Marburg D-35043, Germany;* orcid.org/0000-0002-7573-3191

Xiulan Xie − *Department of Chemistry, University of Marburg, Marburg D-35043, Germany*

Nemanja Djokovic − *Department of Pharmaceutical Chemistry, University of Belgrade, Belgrade 11000, Serbia*

Katarina Nikolic − *Department of Pharmaceutical Chemistry, University of Belgrade, Belgrade 11000, Serbia*

Dmitri Kosenkov − *Department of Chemistry and Physics, Monmouth University, West Long Branch, New Jersey 07764, United States;* orcid.org/0000-0003-0187-3308

Complete contact information is available at: https://pubs.acs.org/10.1021/jacs.3c03275

Funding

D.K. acknowledges the National Science Foundation (NSF, CHE-1955649 RUI-D3S) grant. N.D. and K.N. acknowledge the Ministry of Science and Technological Development of the Republic of Serbia, Faculty of Pharmacy UB Contract No. 451-03-68/2022-14/200161. Numerical simulations were run on the PARADOX-IV supercomputing facility at the Scientific Computing Laboratory, National Center of Excellence for the Study of Complex Systems, Institute of Physics Belgrade, supported in part by the Ministry of Education, Science, and Technological Development of the Republic of Serbia under project no. ON171017. Finally, this work was partially financially supported by the German Research Council (DFG; AB 792/1-1 for F.A. and SPP1926 "Next Generation Optogenetics": 61502867 DFG; VA1002/4-1 for O.V.).

Notes

The authors declare no competing financial interest.

ACKNOWLEDGMENTS

We thank Prof. Dr. E. Meggers for the access to the cell laboratory. D.K. and O.V. thank Research Corporation for Science Advancement and Fulbright German Commission for the Cottrell Scholar Award and the Cottrell Scholar Fulbright Award, respectively.

REFERENCES

(1) Connelly, C. M.; Moon, M. H.; Schneekloth, J. S. Jr., The Emerging Role of RNA as a Therapeutic Target for Small Molecules. *Cell Chem. Biol.* 2016, 23 (9), 1077−1090.

(2) Cooper, T. A.; Wan, L.; Dreyfuss, G. RNA and disease. *Cell* **2009**, *136* (4), 777−93.
(3) Harries, L. W. RNA Biology Provides New Therapeutic Targets for Human Disease. *Front Genet* **2019**, *10*, 205.
(4) Stellos, K. RNA in the spotlight: the dawn of RNA therapeutics in the treatment of human disease. *Cardiovasc. Res.* **2017**, *113* (12), No. e43-e44.
(5) You, M.; Jaffrey, S. R. Designing optogenetically controlled RNA for regulating biological systems. *Ann. N.Y. Acad. Sci.* **2015**, *1352*, 13−9.
(6) Jaschke, A. Genetically encoded RNA photoswitches as tools for the control of gene expression. *FEBS Lett.* **2012**, *586* (15), 2106−11.
(7) Ankenbruck, N.; Courtney, T.; Naro, Y.; Deiters, A. Optochemical Control of Biological Processes in Cells and Animals. *Angew. Chem., Int. Ed. Engl.* **2018**, *57* (11), 2768−2798.
(8) Brieke, C.; Rohrbach, F.; Gottschalk, A.; Mayer, G.; Heckel, A. Light-controlled tools. *Angew. Chem., Int. Ed. Engl.* **2012**, *51* (34), 8446−76.
(9) Berdnikova, D. V. Photoswitches for controllable RNA binding: a future approach in the RNA-targeting therapy. *Chem. Commun. (Camb)* **2021**, *57* (83), 10819−10826.
(10) Asanuma, H.; Liu, M.; Tamaru, D.; Liang, X.; Komiyama, M. Photo-regulation of transcription by RNA polymerase with azobenzene-tethered promoter. *Nucleic Acids Res. Suppl* **2002**, *2* (2), 75−6.
(11) Stafforst, T.; Hilvert, D. Modulating PNA/DNA hybridization by light. *Angew. Chem., Int. Ed. Engl.* **2010**, *49* (51), 9998−10001.
(12) Kamiya, Y.; Takagi, T.; Ooi, H.; Ito, H.; Liang, X.; Asanuma, H. Synthetic gene involving azobenzene-tethered T7 promoter for the photocontrol of gene expression by visible light. *ACS Synth. Biol.* **2015**, *4* (4), 365−70.
(13) Goldau, T.; Murayama, K.; Brieke, C.; Steinwand, S.; Mondal, P.; Biswas, M.; Burghardt, I.; Wachtveitl, J.; Asanuma, H.; Heckel, A. Reversible photoswitching of RNA hybridization at room temperature with an azobenzene C-nucleoside. *Chemistry* **2015**, *21* (7), 2845−54.
(14) Szymanski, W.; Beierle, J. M.; Kistemaker, H. A.; Velema, W. A.; Feringa, B. L. Reversible photocontrol of biological systems by the incorporation of molecular photoswitches. *Chem. Rev.* **2013**, *113* (8), 6114−78.
(15) Zhang, L.; Linden, G.; Vazquez, O. In search of visible-light photoresponsive peptide nucleic acids (PNAs) for reversible control of DNA hybridization. *Beilstein J. Org. Chem.* **2019**, *15*, 2500−2508.
(16) Tang, X.; Swaminathan, J.; Gewirtz, A. M.; Dmochowski, I. J. Regulating gene expression in human leukemia cells using light-activated oligodeoxynucleotides. *Nucleic Acids Res.* **2007**, *36* (2), 559−69.
(17) Deiters, A.; Garner, R. A.; Lusic, H.; Govan, J. M.; Dush, M.; Nascone-Yoder, N. M.; Yoder, J. A. Photocaged morpholino oligomers for the light-regulation of gene function in zebrafish and Xenopus embryos. *J. Am. Chem. Soc.* **2010**, *132* (44), 15644−50.
(18) Shestopalov, I. A.; Sinha, S.; Chen, J. K. Light-controlled gene silencing in zebrafish embryos. *Nat. Chem. Biol.* **2007**, *3* (10), 650−1.
(19) Lotz, T. S.; Halbritter, T.; Kaiser, C.; Rudolph, M. M.; Kraus, L.; Groher, F.; Steinwand, S.; Wachtveitl, J.; Heckel, A.; Suess, B. A light-responsive RNA aptamer for an azobenzene derivative. *Nucleic Acids Res.* **2019**, *47* (4), 2029−2040.
(20) Rotstan, K. A.; Abdelsayed, M. M.; Passalacqua, L. F.; Chizzolini, F.; Sudarshan, K.; Chamberlin, A. R.; Misek, J.; Luptak, A. Regulation of mRNA translation by a photoriboswitch. *Elife* **2020**, *9*, No. e51737.
(21) Weber, A. M.; Kaiser, J.; Ziegler, T.; Pilsl, S.; Renzl, C.; Sixt, L.; Pietruschka, G.; Moniot, S.; Kakoti, A.; Juraschitz, M.; Schrottke, S.; Lledo Bryant, L.; Steegborn, C.; Bittl, R.; Mayer, G.; Moglich, A. A blue light receptor that mediates RNA binding and translational regulation. *Nat. Chem. Biol.* **2019**, *15* (11), 1085−1092.
(22) Pilsl, S.; Morgan, C.; Choukeife, M.; Moglich, A.; Mayer, G. Optoribogenetic control of regulatory RNA molecules. *Nat. Commun.* **2020**, *11* (1), 4825.
(23) Liu, R.; Yang, J.; Yao, J.; Zhao, Z.; He, W.; Su, N.; Zhang, Z.; Zhang, C.; Zhang, Z.; Cai, H.; Zhu, L.; Zhao, Y.; Quan, S.; Chen, X.; Yang, Y. Optogenetic control of RNA function and metabolism using engineered light-switchable RNA-binding proteins. *Nat. Biotechnol.* **2022**, *40* (5), 779−786.
(24) Iijima, T.; Hidaka, C.; Iijima, Y. Spatio-temporal regulations and functions of neuronal alternative RNA splicing in developing and adult brains. *Neurosci Res.* **2016**, *109*, 1−8.
(25) Hemphill, J.; Liu, Q.; Uprety, R.; Samanta, S.; Tsang, M.; Juliano, R. L.; Deiters, A. Conditional control of alternative splicing through light-triggered splice-switching oligonucleotides. *J. Am. Chem. Soc.* **2015**, *137* (10), 3656−62.
(26) Velema, W. A.; Szymanski, W.; Feringa, B. L. Photopharmacology: beyond proof of principle. *J. Am. Chem. Soc.* **2014**, *136* (6), 2178−91.
(27) Borowiak, M.; Kullmer, F.; Gegenfurtner, F.; Peil, S.; Nasufovic, V.; Zahler, S.; Thorn-Seshold, O.; Trauner, D.; Arndt, H. D. Optical Manipulation of F-Actin with Photoswitchable Small Molecules. *J. Am. Chem. Soc.* **2020**, *142* (20), 9240−9249.
(28) Broichhagen, J.; Trauner, D. The in vivo chemistry of photoswitched tethered ligands. *Curr. Opin Chem. Biol.* **2014**, *21*, 121−7.
(29) Hull, K.; Morstein, J.; Trauner, D. In Vivo Photopharmacology. *Chem. Rev.* **2018**, *118* (21), 10710−10747.
(30) Mayer, G.; Heckel, A. Biologically active molecules with a "light switch". *Angew. Chem., Int. Ed. Engl.* **2006**, *45* (30), 4900−21.
(31) Polosukhina, A.; Litt, J.; Tochitsky, I.; Nemargut, J.; Sychev, Y.; De Kouchkovsky, I.; Huang, T.; Borges, K.; Trauner, D.; Van Gelder, R. N.; Kramer, R. H. Photochemical restoration of visual responses in blind mice. *Neuron* **2012**, *75* (2), 271−82.
(32) Pittolo, S.; Gomez-Santacana, X.; Eckelt, K.; Rovira, X.; Dalton, J.; Goudet, C.; Pin, J. P.; Llobet, A.; Giraldo, J.; Llebaria, A.; Gorostiza, P. An allosteric modulator to control endogenous G protein-coupled receptors with light. *Nat. Chem. Biol.* **2014**, *10* (10), 813−5.
(33) Albert, L.; Nagpal, J.; Steinchen, W.; Zhang, L.; Werel, L.; Djokovic, N.; Ruzic, D.; Hoffarth, M.; Xu, J.; Kaspareit, J.; Abendroth, F.; Royant, A.; Bange, G.; Nikolic, K.; Ryu, S.; Dou, Y.; Essen, L. O.; Vazquez, O. Bistable Photoswitch Allows in Vivo Control of Hematopoiesis. *ACS Cent Sci.* **2022**, *8* (1), 57−66.
(34) Borowiak, M.; Nahaboo, W.; Reynders, M.; Nekolla, K.; Jalinot, P.; Hasserodt, J.; Rehberg, M.; Delattre, M.; Zahler, S.; Vollmar, A.; Trauner, D.; Thorn-Seshold, O. Photoswitchable Inhibitors of Microtubule Dynamics Optically Control Mitosis and Cell Death. *Cell* **2015**, *162* (2), 403−411.
(35) Monteys, A. M.; Hundley, A. A.; Ranum, P. T.; Tecedor, L.; Muehlmatt, A.; Lim, E.; Lukashev, D.; Sivasankaran, R.; Davidson, B. L. Regulated control of gene therapies by drug-induced splicing. *Nature* **2021**, *596* (7871), 291−295.
(36) Singh, R. N.; Ottesen, E. W.; Singh, N. N. The First Orally Deliverable Small Molecule for the Treatment of Spinal Muscular Atrophy. *Neurosci Insights* **2020**, *15*, 2633105520973985.
(37) Zhang, L.; Abendroth, F.; Vazquez, O. A Chemical Biology Perspective to Therapeutic Regulation of RNA Splicing in Spinal Muscular Atrophy (SMA). *ACS Chem. Biol.* **2022**, *17* (6), 1293−1307.
(38) Pinard, E.; Green, L.; Reutlinger, M.; Weetall, M.; Naryshkin, N. A.; Baird, J.; Chen, K. S.; Paushkin, S. V.; Metzger, F.; Ratni, H. Discovery of a Novel Class of Survival Motor Neuron 2 Splicing Modifiers for the Treatment of Spinal Muscular Atrophy. *J. Med. Chem.* **2017**, *60* (10), 4444−4457.
(39) Qi, H.; CHOI; Soongyu, Dakka; Amal, Karp; et al. *Compounds for Treating Spinal Muscular Atrophy*. U.S. Patent US9586955B2, 2013.
(40) Bleger, D.; Schwarz, J.; Brouwer, A. M.; Hecht, S. o-Fluoroazobenzenes as readily synthesized photoswitches offering nearly quantitative two-way isomerization with visible light. *J. Am. Chem. Soc.* **2012**, *134* (51), 20597−600.

(41) Morstein, J.; Awale, M.; Reymond, J. L.; Trauner, D. Mapping the Azolog Space Enables the Optical Control of New Biological Targets. *ACS Cent Sci.* **2019**, *5* (4), 607−618.
(42) Beharry, A. A.; Woolley, G. A. Azobenzene photoswitches for biomolecules. *Chem. Soc. Rev.* **2011**, *40* (8), 4422−37.
(43) Schroeder, K. T.; Skalicky, J. J.; Greenbaum, N. L. NMR spectroscopy of RNA duplexes containing pseudouridine in supercooled water. *RNA* **2005**, *11* (7), 1012−6.
(44) Merritt, I. C. D.; Jacquemin, D.; Vacher, M. cis -> trans photoisomerisation of azobenzene: a fresh theoretical look. *Phys. Chem. Chem. Phys.* **2021**, *23* (35), 19155−19165.
(45) Conti, I.; Garavelli, M.; Orlandi, G. The different photoisomerization efficiency of azobenzene in the lowest n pi* and pi pi* singlets: the role of a phantom state. *J. Am. Chem. Soc.* **2008**, *130* (15), 5216−30.
(46) Ootani, Y.; Satoh, K.; Nakayama, A.; Noro, T.; Taketsugu, T. Ab initio molecular dynamics simulation of photoisomerization in azobenzene in the n pi* state. *J. Chem. Phys.* **2009**, *131* (19), 194306.
(47) Aleotti, F.; Soprani, L.; Nenov, A.; Berardi, R.; Arcioni, A.; Zannoni, C.; Garavelli, M. Multidimensional Potential Energy Surfaces Resolved at the RASPT2 Level for Accurate Photoinduced Isomerization Dynamics of Azobenzene. *J. Chem. Theory Comput* **2019**, *15* (12), 6813−6823.
(48) Cembran, A.; Bernardi, F.; Garavelli, M.; Gagliardi, L.; Orlandi, G. On the mechanism of the cis-trans isomerization in the lowest electronic states of azobenzene: S0, S1, and T1. *J. Am. Chem. Soc.* **2004**, *126* (10), 3234−43.
(49) Chang, C. W.; Lu, Y. C.; Wang, T. T.; Diau, E. W. Photoisomerization dynamics of azobenzene in solution with S1 excitation: a femtosecond fluorescence anisotropy study. *J. Am. Chem. Soc.* **2004**, *126* (32), 10109−18.
(50) Crecca, C. R.; Roitberg, A. E. Theoretical study of the isomerization mechanism of azobenzene and disubstituted azobenzene derivatives. *J. Phys. Chem. A* **2006**, *110* (26), 8188−203.
(51) Diau, E. W.-G. A New Trans-to-Cis Photoisomerization Mechanism of Azobenzene on the S1(n,π^*) Surface. *J. Phys. Chem. A* **2004**, *108*, 950−956.
(52) Tang, Z.; Akhter, S.; Ramprasad, A.; Wang, X.; Reibarkh, M.; Wang, J.; Aryal, S.; Thota, S. S.; Zhao, J.; Douglas, J. T.; Gao, P.; Holmstrom, E. D.; Miao, Y.; Wang, J. Recognition of single-stranded nucleic acids by small-molecule splicing modulators. *Nucleic Acids Res.* **2021**, *49* (14), 7870−7883.
(53) Wang, J.; Schultz, P. G.; Johnson, K. A. Mechanistic studies of a small-molecule modulator of SMN2 splicing. *Proc. Natl. Acad. Sci. U. S. A.* **2018**, *115* (20), No. E4604-E4612.
(54) Campagne, S.; Boigner, S.; Rudisser, S.; Moursy, A.; Gillioz, L.; Knorlein, A.; Hall, J.; Ratni, H.; Clery, A.; Allain, F. H. Structural basis of a small molecule targeting RNA for a specific splicing correction. *Nat. Chem. Biol.* **2019**, *15* (12), 1191−1198.
(55) Howell, M. D.; Singh, N. N.; Singh, R. N. Advances in therapeutic development for spinal muscular atrophy. *Future Med. Chem.* **2014**, *6* (9), 1081−99.
(56) Sivaramakrishnan, M.; McCarthy, K. D.; Campagne, S.; Huber, S.; Meier, S.; Augustin, A.; Heckel, T.; Meistermann, H.; Hug, M. N.; Birrer, P.; Moursy, A.; Khawaja, S.; Schmucki, R.; Berntenis, N.; Giroud, N.; Golling, S.; Tzouros, M.; Banfai, B.; Duran-Pacheco, G.; Lamerz, J.; Hsiu Liu, Y.; Luebbers, T.; Ratni, H.; Ebeling, M.; Clery, A.; Paushkin, S.; Krainer, A. R.; Allain, F. H.; Metzger, F. Binding to SMN2 pre-mRNA-protein complex elicits specificity for small molecule splicing modifiers. *Nat. Commun.* **2017**, *8* (1), 1476.
(57) Roca, X.; Krainer, A. R. Recognition of atypical 5′ splice sites by shifted base-pairing to U1 snRNA. *Nat. Struct Mol. Biol.* **2009**, *16* (2), 176−82.
(58) Singh, N. N.; Androphy, E. J.; Singh, R. N. In vivo selection reveals combinatorial controls that define a critical exon in the spinal muscular atrophy genes. *RNA* **2004**, *10* (8), 1291−305.
(59) Singh, N. N.; Singh, R. N.; Androphy, E. J. Modulating role of RNA structure in alternative splicing of a critical exon in the spinal muscular atrophy genes. *Nucleic Acids Res.* **2006**, *35* (2), 371−89.
(60) Yan, Y.; Wang, X.; Chen, J. I.; Ginger, D. S. Photoisomerization quantum yield of azobenzene-modified DNA depends on local sequence. *J. Am. Chem. Soc.* **2013**, *135* (22), 8382−7.
(61) Zhang, M. L.; Lorson, C. L.; Androphy, E. J.; Zhou, J. An in vivo reporter system for measuring increased inclusion of exon 7 in SMN2 mRNA: potential therapy of SMA. *Gene Ther.* **2001**, *8* (20), 1532−8.
(62) Cheung, A. K.; Hurley, B.; Kerrigan, R.; Shu, L.; Chin, D. N.; Shen, Y.; O'Brien, G.; Sung, M. J.; Hou, Y.; Axford, J.; Cody, E.; Sun, R.; Fazal, A.; Fridrich, C.; Sanchez, C. C.; Tomlinson, R. C.; Jain, M.; Deng, L.; Hoffmaster, K.; Song, C.; Van Hoosear, M.; Shin, Y.; Servais, R.; Towler, C.; Hild, M.; Curtis, D.; Dietrich, W. F.; Hamann, L. G.; Briner, K.; Chen, K. S.; Kobayashi, D.; Sivasankaran, R.; Dales, N. A. Discovery of Small Molecule Splicing Modulators of Survival Motor Neuron-2 (SMN2) for the Treatment of Spinal Muscular Atrophy (SMA). *J. Med. Chem.* **2018**, *61* (24), 11021−11036.
(63) Degorce, F.; Card, A.; Soh, S.; Trinquet, E.; Knapik, G. P.; Xie, B. HTRF: A technology tailored for drug discovery - a review of theoretical aspects and recent applications. *Curr. Chem. Genomics* **2009**, *3*, 22−32.
(64) Naryshkin, N. A.; Weetall, M.; Dakka, A.; Narasimhan, J.; Zhao, X.; Feng, Z.; Ling, K. K.; Karp, G. M.; Qi, H.; Woll, M. G.; Chen, G.; Zhang, N.; Gabbeta, V.; Vazirani, P.; Bhattacharyya, A.; Furia, B.; Risher, N.; Sheedy, J.; Kong, R.; Ma, J.; Turpoff, A.; Lee, C. S.; Zhang, X.; Moon, Y. C.; Trifillis, P.; Welch, E. M.; Colacino, J. M.; Babiak, J.; Almstead, N. G.; Peltz, S. W.; Eng, L. A.; Chen, K. S.; Mull, J. L.; Lynes, M. S.; Rubin, L. L.; Fontoura, P.; Santarelli, L.; Haehnke, D.; McCarthy, K. D.; Schmucki, R.; Ebeling, M.; Sivaramakrishnan, M.; Ko, C. P.; Paushkin, S. V.; Ratni, H.; Gerlach, I.; Ghosh, A.; Metzger, F. Motor neuron disease. SMN2 splicing modifiers improve motor function and longevity in mice with spinal muscular atrophy. *Science* **2014**, *345* (6197), 688−93.
(65) England, C. G.; Ehlerding, E. B.; Cai, W. NanoLuc: A Small Luciferase Is Brightening Up the Field of Bioluminescence. *Bioconjug Chem.* **2016**, *27* (5), 1175−1187.
(66) Control NanoLuc Reporter Vector with Hygromycin Selection. https://www.promega.de/products/luciferase-assays/genetic-reporter-vectors-and-cell-lines/control-nanoluc-reporter-vector-with-hygromycin-selection/?catNum=N1411 (accessed 2023−05−19).
(67) Rechsteiner, M. PEST sequences are signals for rapid intracellular proteolysis. *Semin Cell Biol.* **1990**, *1* (6), 433−40.
(68) Scotti, M. M.; Swanson, M. S. RNA mis-splicing in disease. *Nat. Rev. Genet* **2016**, *17* (1), 19−32.
(69) Boer, R. E.; Torrey, Z. R.; Schneekloth, J. S., Jr Chemical Modulation of Pre-mRNA Splicing in Mammalian Systems. *ACS Chem. Biol.* **2020**, *15* (4), 808−818.